Gamma-ray observations of cosmic nuclei

Roland Diehl[1,2,*]

[1]Max Planck Institut für extraterrestrische Physik, D-85748 Garching, Germany
[2]Excellence Cluster 'Origins' and Technical University of Munich, D-85748 Garching, Germany

Abstract. Gamma rays from nuclear processes such as radioactive decay and de-excitations are among the most-direct tools to witness the production and existence of specific nuclei and isotopes in and near cosmic nucleosynthesis sites. With space-borne instrumentation such as NuSTAR and SPI/INTEGRAL, and experimental techniques to handle a substantial instrumental background from cosmic-ray activations of the spacecraft and instrument, unique results have been obtained, from diffuse emissions of nuclei and positrons in interstellar surroundings of sources, as well as from observations of cosmic explosions and their radioactive afterglows. These witness non-sphericity in supernova explosions and a flow of nucleosynthesis ejecta through superbubbles as common source environments. Next-generation experiments that are awaiting space missions promise a next level of observational nuclear astrophysics.

1 Introduction

Observations of gamma rays from nuclear processes are one of the most-direct tools to witness the production and existence of specific nuclei and isotopes in and near cosmic nucleosynthesis sites. Processes that cause characteristic gamma-ray lines from specific nuclides are radioactive decay and energetic collisions, both resulting in de-excitations of specific (daughter-) isotopes. Observations in the gamma-ray band require space-borne instrumentation, because the atmosphere of the Earth presents a thick target to gamma rays and their interactions with nuclei and electrons[1] In this paper, we will briefly address the required instrumentation and analysis methods, and then review what has been learned from diffuse emissions of nuclei in interstellar surroundings of sources, as well as from observations of cosmic explosions and their radioactive afterglows.

2 Telescopes for nuclear line emissions

Space-borne instrumentation are a technical challenge, as they must be built to survive their launch into space, and operations in a harsh environment characterised by high irradiation from cosmic rays and extreme temperature gradients between sun-exposed components and

*e-mail: rod@mpe.mpg.de

[1]This is exploited for ground based gamma-ray astronomy at TeV energies and above, using the atmosphere as a detector, though the electromagnetic shower of particles and photons that is created by high-energy gamma-rays interacting in the atmosphere.

those in the shadow and cold space. Experimental techniques are required to handle a substantial instrumental background in the measured detector events, caused from cosmic-ray activations of the spacecraft and instrument (see [1] for a detailed example).

Successful pioneering sky imaging and spectroscopy surveys with Compton-CGRO [2] and INTEGRAL [3], respectively, have shown the potential of this astronomical window. Currently, only the INTEGRAL and NuSTAR[4] missions are in operation for measurements of nuclear lines from cosmic sources. Both these missions are in their late, extended, phases, and may be terminated soon. No future mission for nuclear astronomy is currently planned by any of the international space agencies [see however 5–7, for recent project proposals and prototypes].

3 Supernova explosions

3.1 Thermonuclear supernovae

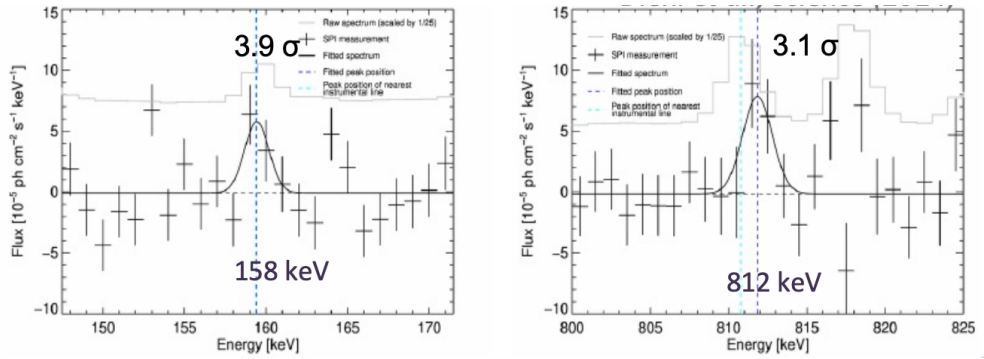

Figure 1. The early detection of decay lines from ^{56}Ni after 20 days past explosion signify appearance of ^{56}Ni at surprisingly-low optical depth [14]. Although the significance is at the 4σ level only, this signifies a deviation from the standard assumption of ^{56}Ni being at the center of a nearly-spherical explosion. The instrumental background spectrum is indicated as grey histogram, scaled down to fit; the nearest instrumental line positions are indicated by dashed lines (green), while the fitted line centers of the SN2014J signal are also indicated (dashed black lines).

Fourty years after their prediction from supernova models [e.g. 8], finally the characteristic ^{56}Co gamma-ray lines from the decay chain of ^{56}Ni could be measured with the INTEGRAL observatory [9] and in particular its gamma-ray spectrometer SPI [10, 11]. Supernova SN2014J was close enough to provide sufficiently-intense gamma-ray flux for this observational proof of a key ingredient of modeling supernova light from thermonuclear supernovae, from ^{56}Co radioactivity with its characteristic 11 day decay time. The amount of ^{56}Ni inferred from the gamma-ray flux of 0.49±0.09 $M_\odot$ [10] is in agreement with the amount inferred from the optical brightness of the supernova, as based on the empirical peak-brightness/^{56}Ni heating-rate relation called *Arnett's law* [12]. This is reassuring.

On the other hand, there were indications in the time series of gamma-ray spectra from the ^{56}Co decay lines that individual clumps of ^{56}Co decay at different bulk velocities appeared at different times, signifying substantial deviations from spherical symmetry of explosion or ^{56}Co distribution [see 10, for more detail on the ^{56}Co gamma-ray signal]. Even more clear and spectacular was the detection of ^{56}Ni decay lines early-on (Fig. 1): With a radioactive lifetime

of about 9 days, it was believed that ^{56}Ni would always be embedded so deeply within the supernova's core that even gamma-rays could not leak out before ^{56}Ni was converted to ^{56}Co already. Only some *He cap* models included the possibility of early gamma-ray emission from ^{56}Ni decay [13], as helium deposition on the surface of the white dwarf could cause a helium surface explosion triggering the thermonuclear supernova. Thus, this discovery of early ^{56}Ni gamma-ray lines was discussed as a support for such a double detonation [see 14, for more detail], and double-degenerate progenitor models in general.

3.2 Core-collapse supernovae

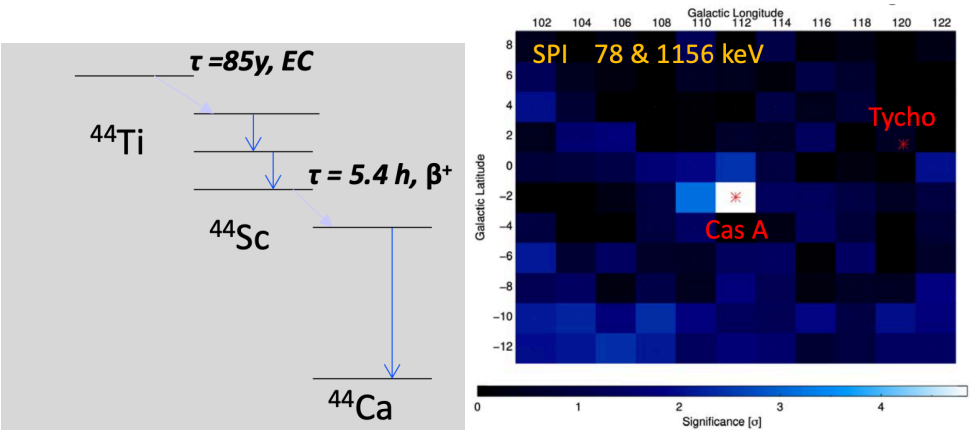

Figure 2. *Left:* The signal of ^{44}Ti decay results in lines at 68, 78, and 1156 keV. *Right:* The SPI ^{44}Ti line signal is clearly attributed to the Cas A source (right). [From 15].

SN1987A still is the core-collapse supernova with best observational details of the aftermath of such an explosion of a massive star after its gravitational collapse. However, the Cas A supernova remnant comes close in that impressive observational detail of the supernova remnant at its young age of about 350 years allows for interpretations and tests of our supernova explosion models in great detail. At this age, the energy input to the supernova remnant from radioactive decay of ^{44}Ti is most important. With its decay time of 89 year, ^{44}Ti decay (see Figure 2 left) provides lines at 68 and 78 keV from the first decay stage, i.e. de-excitations of ^{44}Sc, and another line at 1156 keV from the ^{44}Ca daughter isotope, which had led to its discovery with the COMPTEL instrument [16]. NuSTAR with its imaging hard X-ray telescope can observe the two low-energy lines from ^{44}Ti decay, and the image derived from these observations has been an illuminating lesson for us [17, 18]. The image shows several clumps of ^{44}Ti emission in the central region of the remnant, and imaging-resolved spectroscopy demonstrates that among these clumps different bulk velocities can be discriminated. But in spite of its technological advantages with hard-X-ray optics, also NuSTAR detector signals suffer from a large background, from a diffuse cosmic X-ray background and from cosmic-rays that activate spacecraft materials and lead to a large instrumental background. Independent measurements with other instruments are important to address potential systematics in such data analyses, as they are dependent on models for instrumental backgrounds and response behaviour. INTEGRAL/SPI conducted a deep observational campaign to provide high-quality data for Cas A, accumulated now to 11.2 Ms of exposure.

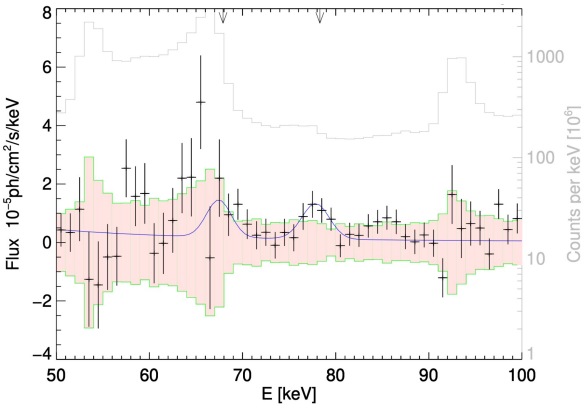

Figure 3. The signal of lines from ^{44}Sc de-excitation in Cas A is shown here, together with uncertainties remaining from the instrumental background model (redish hatched area). The instrumental background shape is shown as a histogram in grey. [From 15].

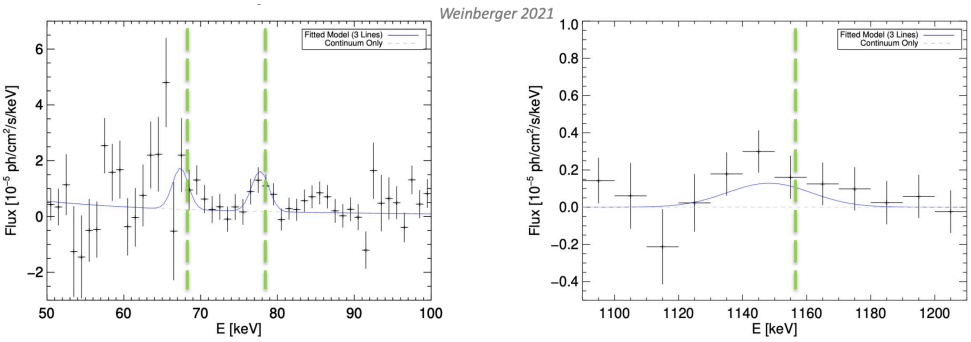

Figure 4. The signal in all lines from ^{44}Ti in Cas A show a bulk redshift (dashed lines mark the laboratory values of the respective line energies. [From 15].

Figure 2 (right) shows from this analysis [19] that the ^{44}Ti signal in SPI spectra can safely be attributed to the Cas A source, rather than diffuse emission or another nearby source. Figure 3 shows the spectrum around the low-energy lines measured also by NuSTAR, indicating the uncertainties incurred by the instrumental background. In Figure 4, we show the latest spectra for the two lines with high-quality signals, i.e., the 78 keV and 1156 keV lines. In both spectra, it is evident that the fitted line energy is offset towards lower energies, which is interpreted as Doppler shift from net bulk motion. The effect is more obvious in teh 1156 keV line, as Doppler shifts scale with photon energy. These spectra independently thus confirm the NuSTAR finding of predominant motion of ^{44}Ti away from us, resulting in a net redshift for all of the observed ^{44}Ti. Note that for SPI on INTEGRAL, Cas A appears as an unresolved point-like source, as imaging resultion with the SPI coded-mask telescope is about 3 degrees only.

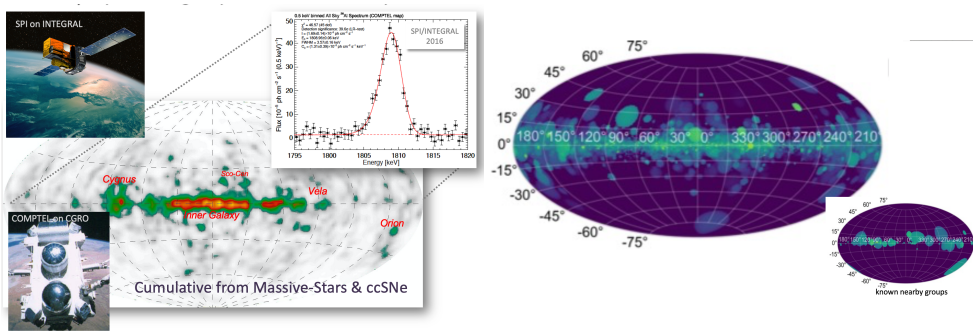

Figure 5. *Left:* The ^{26}Al decay in the Galaxy has been imaged across the sky with data from COMPTEL; high-resolution spectroscopy was added with measurements from INTEGRAL . *Right:* A bottom-up model, based on known massive-star cluster locations nearby and MC-sampled clusters at large distances, and using stellar and supernova yields and line-of-sight integrated intensities, predicts an ^{26}Al appearance of the sky that is close to observations. The inset at the bottom right shows the contributions from known nearby clusters alone. [From 30]

4 Source environments and ejecta flow

More long-live radioactivities, with decay times that exceed the occurrence frequency of nucleosynthesis events that may eject those, will accumulate in the interstellar medium around the sources. These will appear as diffuse emission, from the neighbourhood of sources. For lifetimes longer than the mixing timescale of the interstellar medium, which is estimated to be around 100 Myrs, only diffuse extended or large-scale emission will signify such nucleosynthesis, and no astronomical information is retained. But for lifetimes between 0.1 and several Myrs, one may expect to be able to trace the flow of nucleosynthesis ejecta on their early path from the sources towards spreading in the general galactic interstellar medium, before cooling down to be able to form clouds and stars of a next generation herein. ^{26}Al and ^{60}Fe , with radioactive lifetimes of 1.04 and 3.8 Myrs, repsectively, are suited for such tracing of ejecta flows, once their radioactivity gamma-ray lines can be measured with adequate significance.

4.1 Diffuse ^{26}Al emission of the Galaxy

The gamma-ray line from ^{26}Al decay has first been measured in 1978 [20], and has been imaged across the sky from data of the NASA Compton Observatory and its COMPTEL instrument (Figure 5 left, [21, 22]. From the image, it had been clear that massive-star groups and their supernovae were the most plausible sources [23]. INTEGRAL's gamma-ray spectrometer had adequate energy resolution to add spectroscopic information on ^{26}Al (Figure 5 left, [24–27]) (SPI resolution 2-3 keV, versus 200 keV for COMPTEL).

One of the key results derived from these observations has been the rate of core-collapse supernovae within our Galaxy [25]. This is based on the measured ^{26}Al line flux, and its interpretations along the line of sight in terms of an adopted source distribution model for our Galaxy, to infer the absolute amount of ^{26}Al within our Galaxy. Using yields from supernova and massive-star models, plus an adopted distribution of stars across their entire mass range (i.e., from 8-10 to about 120 $M_\odot$), one can then determine a supernova rate, that is based on a Galaxy-wide measurement (as opposed to measurements of massive-star census in the solar

vicinity with extrapolation, or measurements of galaxies other than our Milky Way Galaxy; [see 25, for a discussion].

Originally, we adopted a first-order Galactic-structure model in the form of a double-exponential disk, with scale parameters galactocentric radius $R_{disk} = 4$ kpc and scale height $z_{disk} = 0.18$ kpc, as found to be an acceptable fit for the inner Galaxy region $-30^0 \leq l \leq 30^0$ degrees and $-10^0 \leq b \leq 10^0$ degrees. We found that other spatial models such as spiral arm models and models with plausibly well-fitting scale heights in the range 100-400 pc did alter the result by less than 4%.

We have recently deepened our investigations of the first step in this analysis, i.e., the determination of the ^{26}Al flux and its allocation to sources along the line of sight. Thus, we expanded the region used for this analysis from 'inner-Galaxy only' to 'all sky'. Then, we used our results from fitting a variety of massive-star tracers in the Galaxy [see 26, 28, 29, for details on tracer fitting] to better constrain sources along lines of sight by knowledge about our Galaxy and in particular the vicinity of the solar system. The ^{26}Al flux measurement can be extended to the entire sky and to the use of both single and multiple events in SPI's germanium detectors [30]. The latter requires careful modeling of instrumental backgrounds, following the directives of our studies of instrumental background and response behaviour [1, 31]. For a reliable flux determination using the entire sky, imaging deconvolution and the integration of deconvolved flux in the image may appear as a straightforward method. However, as the instrumental response is complex for gamma-ray instruments and far from merely a somewhat blurred point spread function, and the Poissonian noise from a high intensity of background counts is severe, such deconvolutions require iterative revisions of forward-convolved model using maximum-likelihood criteria for determination of their parameters. The resulting images therefore are biased from the way models have been constructed [see 32, for a detailed discussion of these issues for the case of the COMPTEL telescope]. In the end, for best flux determination one must find a spatial model that is satisfactory in terms of goodness of fit and in terms of what we know about ^{26}Al sources and about their candidate tracers in the neighbourhood of the solar system and out to large lines of sight through our Galaxy. This is based on catalogues of massive stars and massive-star clusters for the distances out to which those are reliable [30]. Then, these were combined with a population synthesis approach [following 33], and adopting some spatial blurring from ^{26}Al propagation within a cluster's age, to derive a *bottom-up* expectation for ^{26}Al emission from the massive-star groups in the solar neighbourhood; these are most important for the flux determination as flux scales with $\frac{1}{distance^2}$. Figure 5, right, shows the contribution from these nearby clusters in the lower-right part of the image. Then, Monte-Carlo sampling of candidate massive star clusters was used for the more-distant part of the Galaxy [30] , drawing from a Galaxy model as before. Now, this part of spatial modeling was then used only for the part of the Galaxy where other information is not available. Comparing results for a variety of tracers commonly used for massive stars, starting from exponential disks of different sizes, then different spiral-arm based models were used [30], all with scale heights in the potential range of interest as found for ^{26}Al data scale height fitting [26]. Finally, this population synthesis modeling determines expected ^{26}Al fluxes using yields from models of massive stars and core-collapse supernovae, and an appropriate mass range and mass weighting. The latter includes different initial-mass functions for massive stars, and different supernova explodability models [see 30, for details]. Globally, yields then are scaled with a star formation rate factor for the entire Galaxy. Figure 5, right, displays the morphology of the ^{26}Al sky as composed from such a *bottom-up* modeling effort, for one set of plausible parameters.

One result from these studies is that the total mass of ^{26}Al in our Galaxy is reduced by as much as 25 to 30%; this is due to a better account of nearby source regions, such as the Scorpius-Centaurus stars or other groups out kpc distances such as in the Cygnus region.

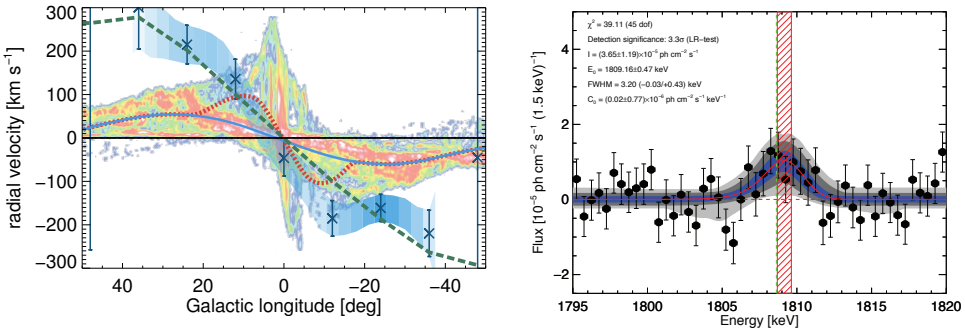

Figure 6. *Left:* The ^{26}Al decay line shows systematic shifts along Galactic longitudes, which are attributed to large scale Galactic rotation [34]. Excess velocities of about 200 km s^{-1} are observed with respect to other tracers of Galactic rotation (colour scale: CO clouds). This is attributed to on-average larger streaming velocities in cavities elongated into the forward direction of galactic rotation [35]. *Right:* ^{26}Al line spectrum from the Orion region, indicating blue shifted emission from bulk motion towards the observer [27].

Thus, plausible Galactic ^{26}Al masses do not exceed 2 $M_\odot$, for plausible values of the star formation rate not exceeding 5 $M_\odot$ y^{-1}. Also, these studies show a remarkable sensitivity to largely-extended ^{26}Al flux from also high-latitude regions, such as could occur if the nearby massive-star groups had produced superbubbles that extend over large regions of the sky; the 'Local Bubble' is one such candidate. All these results [see 30, and Diehl *et al., in preparation*] point into the direction that the rate of core-collapse supernovae derived from ^{26}Al measurements and their modeling will fall into a range of 1.0 to 1.3 century^{-1}, equivalent to a recurrence rate of around 75 years.

4.2 ^{26}Al kinematics and superbubbles

The analysis of the ^{26}Al gamma-ray line and its dependency with viewing directions had led to the finding that systematic line shifts reminiscent of large-scale galactic rotation was observed [25, 34]. Comparing the ^{26}Al data with other tracers of such large-scale Galactic rotation (Figure 6, left), it was evident that ^{26}Al data showed a systematic velocity excess with respect to all other sources. This was understood and modelled as being the result of ^{26}Al propagation within large cavities (superbubbles) that extended asymmetrically around the massive-star clusters at their origins [35] (see green dashed model line in Figure 6, left). Thus, ^{26}Al kinematics results are supportive of our suggestion that massive star nucleosynthesis is preferentially injected into circumstellar surroundings in the form of large superbubbles, that have been blown by winds of the most-massive, hence rapidly-evolving, stars of the clusters, and later increased further by successive supernova explosions within. The density gradient away from spiral arms as the birth sites of these stellar clusters leads to a large extent of these superbubbles towards lower densities in inter-arm regions and the Galactic halo. This allows ^{26}Al that is ejected into directions following the large-scale rotation can propagate for a longer time freely until decay, while ^{26}Al ejcted into the opposite direction will be decelerated by higher density environments such as the back end of the superbubble wall before its radioactive decay, so that decay occurs at a lower velocity; the net effect of this kinematic situation will be a systematic velocity bias in the direction of galactic rotation, as observed.

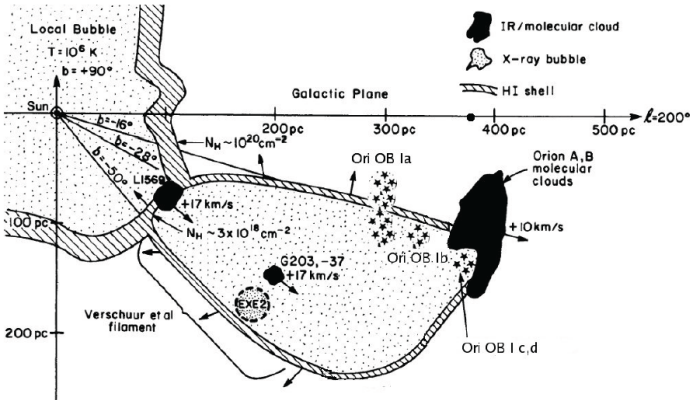

Figure 7. The Orion region is characterised by two massive molecular clouds at about 450 pc distance, with recent massive-star formation preferentially on its near side (star symbols), and a large cavity bounded by denser HI emission, which extends from the clouds towards the direction of the Sun. ([Updated from 37] [by 36].

The Orion region with the Orion A and B molecular clouds at about 450 pc distance and its OB1 association subgroups presents a situation that again supoorts this picture. The Eridanus cavity has been mapped in HI and X rays to extend from the Orion molecular clouds far and asymmetrically towards the Sun, as shown in the sketch of Figure 7 [36]. From the geometry shown, it appears plausible that ^{26}Al emission also should have a velocity bias from such propagation within the Eridanus cavity. INTEGRAL/SPI observations show a tantalizing hint for such a blue shift of the line [27], although not significant in current results (Figure 6, right). More observational data are being accumulated, towards this test of our superbubble picture.

4.3 Diffuse ^{60}Fe emission of the Galaxy

^{60}Fe dffuse gamma-ray line emission had been discovered with RHESSI [38], later also measured with INTEGRAL/SPI [39, 40]. From models of massive-star nucleosynthesis, these sources of ^{26}Al were also expected to eject ^{60}Fe radioactivity at the same time, and with similar amounts [41]. But these observations quickly made clear that ^{60}Fe gamma-ray intensities are well below those of ^{26}Al gamma rays, by as much as a factor of ten. This presents a challenge to astrophysical models of massive stars and their supernovae [see 42, 43, for a thorough discussion].

In an effort to better determine the intensity ratio between ^{26}Al and ^{60}Fe , we analysed both these isotopes from a dataset that included identical observations and data selections, in order to minimize any systematic effects, such as could occur from using slightly different sky exposures or data selections [44]. We found spectral intensities is shown in Figure 8, left, for one plausible sky intensity distribution that may represent both emissions. Their analysis then used a variety of candidate tracers for ^{26}Al and for ^{60}Fe , comparing qualities of the fit to SPI observations. It turned out that morphologies of ^{26}Al and of ^{60}Fe emissions are not necessarily identical, however with clear similarities; ^{60}Fe emission also is plausibly diffuse and extended, rather than originating from very few sources only. From astrophysical models, indeed some differences could be expected. Simulations of simple galaxy models illustrate this [45, 46]. Also, in our population synthesis models [30], differences are found,

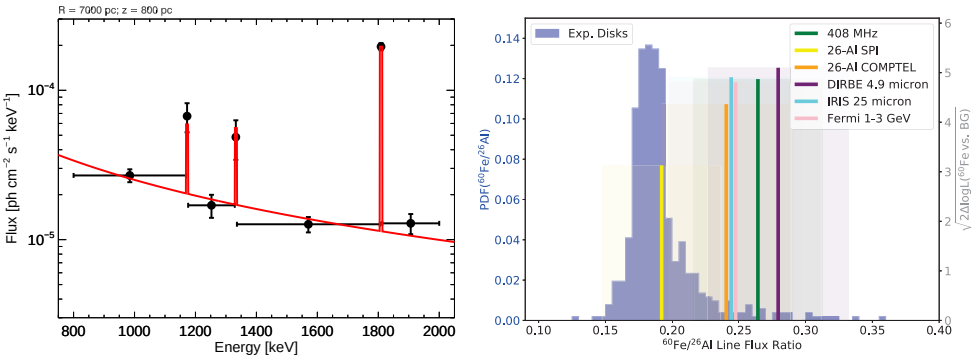

Figure 8. *Left:* The ^{60}Fe signal and ^{26}Al decay line intensities can be compared in INTEGRAL analyses from a consistent set of observations [44]. *Right:* From modeling comparisons using a wide set of different spatial distribution and tracer models, the gamma-ray intensity ratio ^{60}Fe /^{26}Al is constraints to 0.4 as an upper bound . [44].

upon a closer look, although here we adopted the massive-star/core-collapse supernova origin for ^{60}Fe . From this analysis, the total Galactic amount of ^{60}Fe was found to be around 4-6 $M_\odot$ [30]. We studied systematic effects from different modelings of spatial distributions (see Figure 8, right) [44], and concluded that the ^{60}Fe /^{26}Al intensity ratio is constrained to be below a value of 0.4, as an upper limit. As stated above, this is a challenge for current models [see also 30].

5 Conclusions

Gamma-ray lines from cosmic sources of nucleosynthesis have been accessible to observations since more than four decades. Imaging information is limited, as gamma-ray telescopes have fundamental limits in the degree range.

Spectral lines, however, reveal unique details about sources of nucleosynthesis, in particular about supernova explosions. Lines from the ^{56}Ni and ^{44}Ti decay chains have confirmed the fundamental understanding that nucleosynthesis ejecta with radioactive isotopes power the afterglow emission of supernova explosions through their decay gamma rays and leptons. Gamma-ray spectroscopy has also shown that supernova explosions of both types, thermonuclear, and core collapse, are likely not spherically symmetric; data from SN2014J, and from Cas A, respectively, show clear signs of bulk motion deviant from spherical symmetry.

Long-lived radioactive admixtures of nucleosynthesis ejecta in the forms of ^{26}Al and ^{60}Fe have shown that massive-star clusters are prominent sources of these trace isotopes. Analysing the ^{26}Al emission morphology of the Galaxy, and kinematic Doppler information from imaging spectroscopy, it is found that superbubbles of large extents are characteristic environments wherein massive-star ejecta are launched, towards eventually cooling and mixing with ambient gas towards later formation of next-generation stars. ^{60}Fe emission is found considerably fainter than ^{26}Al emission, limited to about 40% of ^{26}Al . It is important to combine these gamma-ray results with other messengers of interstellar gas, to learn how nucleosynthesis ejecta propagate to lead to galactic and cosmic chemical evolution.

Acknowledgements. This work is supported through the Max Planck Society/MPE, through the European COST action number 16117 'ChETEC', the Excellence Clusters 'Universe' and 'Origins', and DLR as well as ESA, supporting the INTEGRAL mission.

References

[1] R. Diehl, T. Siegert, J. Greiner, M. Krause, K. Kretschmer, M. Lang, M. Pleintinger, A.W. Strong, C. Weinberger, X. Zhang, Astron. Astrophys. **611**, A12 (2018)

[2] N. Gehrels, E. Chipman, D.A. Kniffen, Astron. Astrophys. Suppl. **97**, 5 (1993)

[3] C. Winkler, T.J.L. Courvoisier, G. Di Cocco, N. Gehrels, A. Giménez, S. Grebenev, W. Hermsen, J.M. Mas-Hesse, F. Lebrun, N. Lund et al., Astron. Astrophys. **411**, L1 (2003)

[4] F.A. Harrison, W.W. Craig, F.E. Christensen, C.J. Hailey, W.W. Zhang, S.E. Boggs, D. Stern, W.R. Cook, K. Forster, P. Giommi et al., Astrophys. J. **770**, 103 (2013), 1301.7307

[5] A. de Angelis, V. Tatischeff, I.A. Grenier, J. McEnery, M. Mallamaci, M. Tavani, U. Oberlack, L. Hanlon, R. Walter, A. Argan et al., Journal of High Energy Astrophysics **19**, 1 (2018), 1711.01265

[6] T. Tanimori, arXiv e-prints arXiv:2002.05362 (2020), 2002.05362

[7] J.A. Tomsick, S.E. Boggs, A. Zoglauer, E. Wulf, L. Mitchell, B. Phlips, C. Sleator, T. Brandt, A. Shih, J. Roberts et al., arXiv e-prints arXiv:2109.10403 (2021), 2109.10403

[8] D.D. Clayton, S.E. Woosley, Reviews of Modern Physics **46**, 755 (1974)

[9] E. Churazov, R. Sunyaev, J. Isern, J. Knödlseder, P. Jean, F. Lebrun, N. Chugai, S. Grebenev, E. Bravo, S. Sazonov et al., Nature **512**, 406 (2014), 1405.3332

[10] R. Diehl, T. Siegert, W. Hillebrandt, M. Krause, J. Greiner, K. Maeda, F.K. Röpke, S.A. Sim, W. Wang, X. Zhang, Astron. Astrophys. **574**, A72 (2015), 1409.5477

[11] J. Isern, P. Jean, E. Bravo, J. Knödlseder, F. Lebrun, E. Churazov, R. Sunyaev, A. Domingo, C. Badenes, D.H. Hartmann et al., Astron. Astrophys. **588**, A67 (2016), 1602.02918

[12] W.D. Arnett, Astrophys. J. **253**, 785 (1982)

[13] L.S. The, A. Burrows, Astrophys. J. **786**, 141 (2014), 1402.4806

[14] R. Diehl, T. Siegert, W. Hillebrandt, S.A. Grebenev, J. Greiner, M. Krause, M. Kromer, K. Maeda, F. Röpke, S. Taubenberger, Science **345**, 1162 (2014), 1407.3061

[15] C. Weinberger, Ph.D. thesis, TU Munich (2021)

[16] A.F. Iyudin, R. Diehl, H. Bloemen, W. Hermsen, G.G. Lichti, D. Morris, J. Ryan, V. Schoenfelder, H. Steinle, M. Varendorff et al., Astron. Astrophys. **284**, L1 (1994)

[17] B.W. Grefenstette, F.A. Harrison, S.E. Boggs, S.P. Reynolds, C.L. Fryer, K.K. Madsen, D.R. Wik, A. Zoglauer, C.I. Ellinger, D.M. Alexander et al., Nature **506**, 339 (2014), 1403.4978

[18] B.W. Grefenstette, C.L. Fryer, F.A. Harrison, S.E. Boggs, T. DeLaney, J.M. Laming, S.P. Reynolds, D.M. Alexander, D. Barret, F.E. Christensen et al., Astrophys. J. **834**, 19 (2017), 1612.02774

[19] C. Weinberger, R. Diehl, M.M.M. Pleintinger, T. Siegert, J. Greiner, Astron. Astrophys. **638**, A83 (2020), 2004.12688

[20] W.A. Mahoney, J.C. Ling, A.S. Jacobson, R.E. Lingenfelter, Astrophys. J. **262**, 742 (1982)

[21] R. Diehl, Experimental Astronomy **6**, 103 (1995)

[22] S. Plüschke, R. Diehl, V. Schönfelder, H. Bloemen, W. Hermsen, K. Bennett, C. Winkler, M. McConnell, J. Ryan, U. Oberlack et al., *The COMPTEL 1.809 MeV survey*, in *Exploring the Gamma-Ray Universe*, edited by A. Gimenez, V. Reglero, C. Winkler (2001), Vol. 459 of *ESA Special Publication*, pp. 55–58

[23] N. Prantzos, Astron. Astrophys. Suppl. **120**, C303+ (1996)

[24] R. Diehl, K. Kretschmer, S. Plüschke, V. Schönfelder, A.W. Strong, M. Cerviño, D. Hartmann, Astronomische Nachrichten Supplement **324**, 18 (2003)

[25] R. Diehl, N. Prantzos, P. von Ballmoos, Nuclear Physics A **777**, 70 (2006), arXiv:astro-ph/0502324

[26] W. Wang, M.G. Lang, R. Diehl, H. Halloin, P. Jean, J. Knödlseder, K. Kretschmer, P. Martin, J.P. Roques, A.W. Strong et al., Astron. Astrophys. **496**, 713 (2009), 0902.0211

[27] T. Siegert, R. Diehl, *The ^{26}Al Gamma-ray Line from Massive-Star Regions*, in *14th International Symposium on Nuclei in the Cosmos (NIC2016)*, edited by S. Kubono, T. Kajino, S. Nishimura, T. Isobe, S. Nagataki, T. Shima, Y. Takeda (2017), p. 020305, 1609.08817

[28] R. Diehl, K. Bennett, C. Dupraz, J. Knoedlseder, G. Lichti, D. Morris, U. Oberlack, J. Ryan, V. Schoenfelder, A. Strong et al., Astron. Astrophys. Suppl. **120**, C321+ (1996)

[29] J. Knödlseder, K. Bennett, H. Bloemen, R. Diehl, W. Hermsen, U. Oberlack, J. Ryan, V. Schönfelder, P. von Ballmoos, Astron. Astrophys. **344**, 68 (1999)

[30] M.M.M. Pleintinger, Ph.D. thesis, Technische Universität München (2020)

[31] T. Siegert, R. Diehl, C. Weinberger, M.M.M. Pleintinger, J. Greiner, X. Zhang, Astron. Astrophys. **626**, A73 (2019), 1903.01096

[32] J. Knödlseder, D. Dixon, K. Bennett, H. Bloemen, R. Diehl, W. Hermsen, U. Oberlack, J. Ryan, V. Schönfelder, P. von Ballmoos, Astron. Astrophys. **345**, 813 (1999), arXiv:astro-ph/9903172

[33] R. Voss, R. Diehl, D.H. Hartmann, M. Cerviño, J.S. Vink, G. Meynet, M. Limongi, A. Chieffi, Astron. Astrophys. **504**, 531 (2009), 0907.5209

[34] K. Kretschmer, R. Diehl, M. Krause, A. Burkert, K. Fierlinger, O. Gerhard, J. Greiner, W. Wang, Astron. Astrophys. **559**, A99 (2013), 1309.4980

[35] M.G.H. Krause, R. Diehl, Y. Bagetakos, E. Brinks, A. Burkert, O. Gerhard, J. Greiner, K. Kretschmer, T. Siegert, Astron. Astrophys. **578**, A113 (2015), 1504.03120

[36] K.M. Fierlinger, A. Burkert, E. Ntormousi, P. Fierlinger, M. Schartmann, A. Ballone, M.G.H. Krause, R. Diehl, Mon. Notices Royal Astron. Soc. **456**, 710 (2016), 1511.05151

[37] D.N. Burrows, K.P. Singh, J.A. Nousek, G.P. Garmire, J. Good, Astrophys. J. **406**, 97 (1993)

[38] D.M. Smith, *Gamma-Ray Line Observations with RHESSI*, in *5th INTEGRAL Workshop on the INTEGRAL Universe*, edited by V. Schoenfelder, G. Lichti, C. Winkler (2004), Vol. 552 of *ESA Special Publication*, pp. 45–+

[39] M.J. Harris, J. Knödlseder, P. Jean, E. Cisana, R. Diehl, G.G. Lichti, J.P. Roques, S. Schanne, G. Weidenspointner, Astron. Astrophys. **433**, L49 (2005), arXiv:astro-ph/0502219

[40] W. Wang, M.J. Harris, R. Diehl, H. Halloin, B. Cordier, A.W. Strong, K. Kretschmer, J. Knödlseder, P. Jean, G.G. Lichti et al., Astron. Astrophys. **469**, 1005 (2007), 0704.3895

[41] F.X. Timmes, S.E. Woosley, D.H. Hartmann, R.D. Hoffman, T.A. Weaver, F. Matteucci, Astrophys. J. **449**, 204 (1995), arXiv:astro-ph/9503120

[42] R. Diehl, M.G.H. Krause, K. Kretschmer, M. Lang, M.M.M. Pleintinger, T. Siegert, W. Wang, L. Bouchet, P. Martin, New Astron. Rev. **92**, 101608 (2021), 2011.06369

[43] R. Diehl, M. Lugaro, A. Heger, A. Sieverding, X. Tang, K. Li, E. Li, C.L. Doherty, M.G.H. Krause, A. Wallner et al., arXiv e-prints arXiv:2109.08558 (2021),

2109.08558

[44] W. Wang, T. Siegert, Z.G. Dai, R. Diehl, J. Greiner, A. Heger, M. Krause, M. Lang, M.M.M. Pleintinger, X.L. Zhang, Astrophys. J. **889**, 169 (2020), 1912.07874

[45] Y. Fujimoto, M.R. Krumholz, S. Tachibana, Mon. Notices Royal Astron. Soc. **480**, 4025 (2018), 1802.08695

[46] D. Rodgers-Lee, M.G.H. Krause, J. Dale, R. Diehl, Mon. Notices Royal Astron. Soc. **490**, 1894 (2019), 1909.10978